In-gas-jet laser spectroscopy of Er with S^3-LEB

Wenling Dong

IJCLab

May 29, 2024

Outline

- Off-line laser spectroscopy of Er with S^3-LEB
- Analysis
  - Isotope shift
  - Broadening mechanisms of spectral lines
  - Hyperfine structure
- Conclusion and outlook

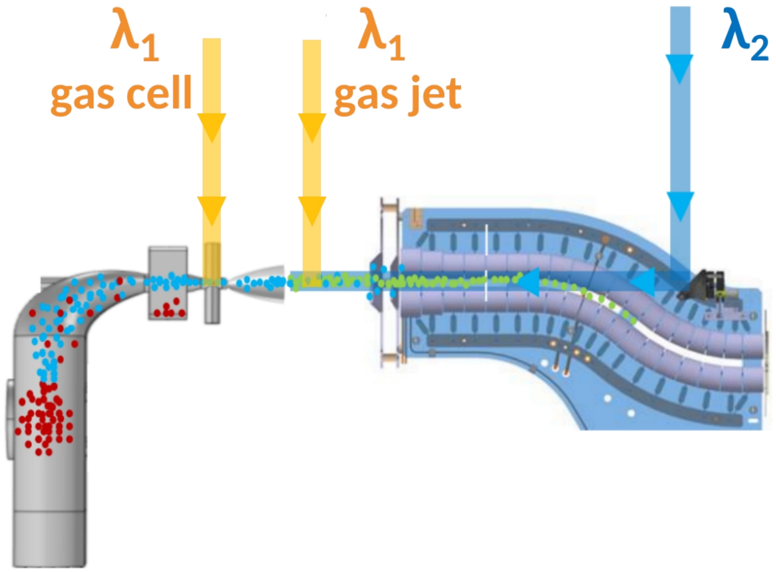

S^3-LEB setup

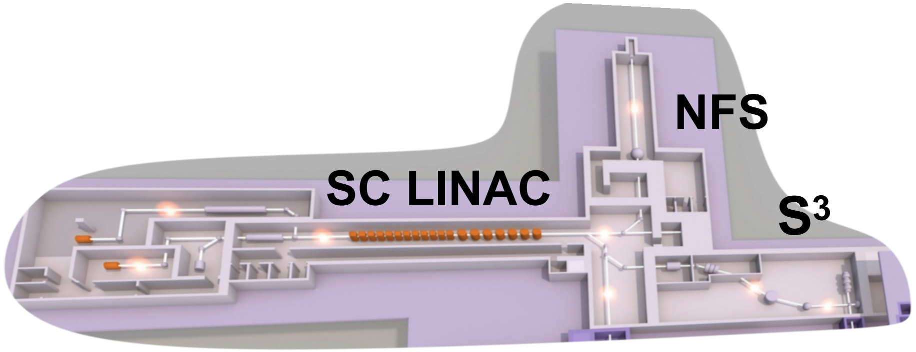

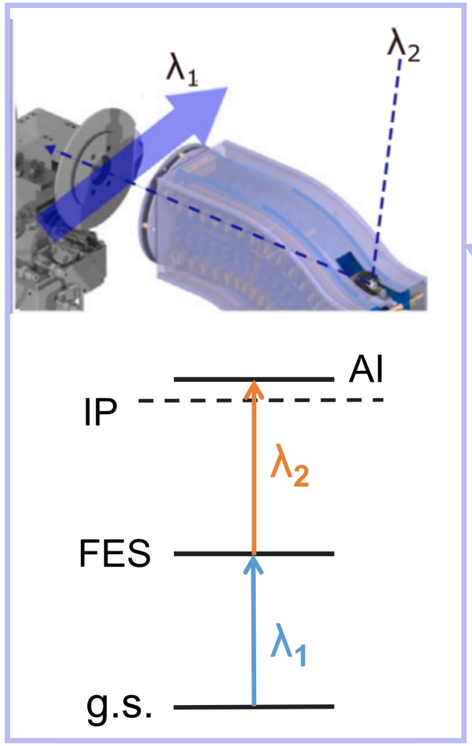

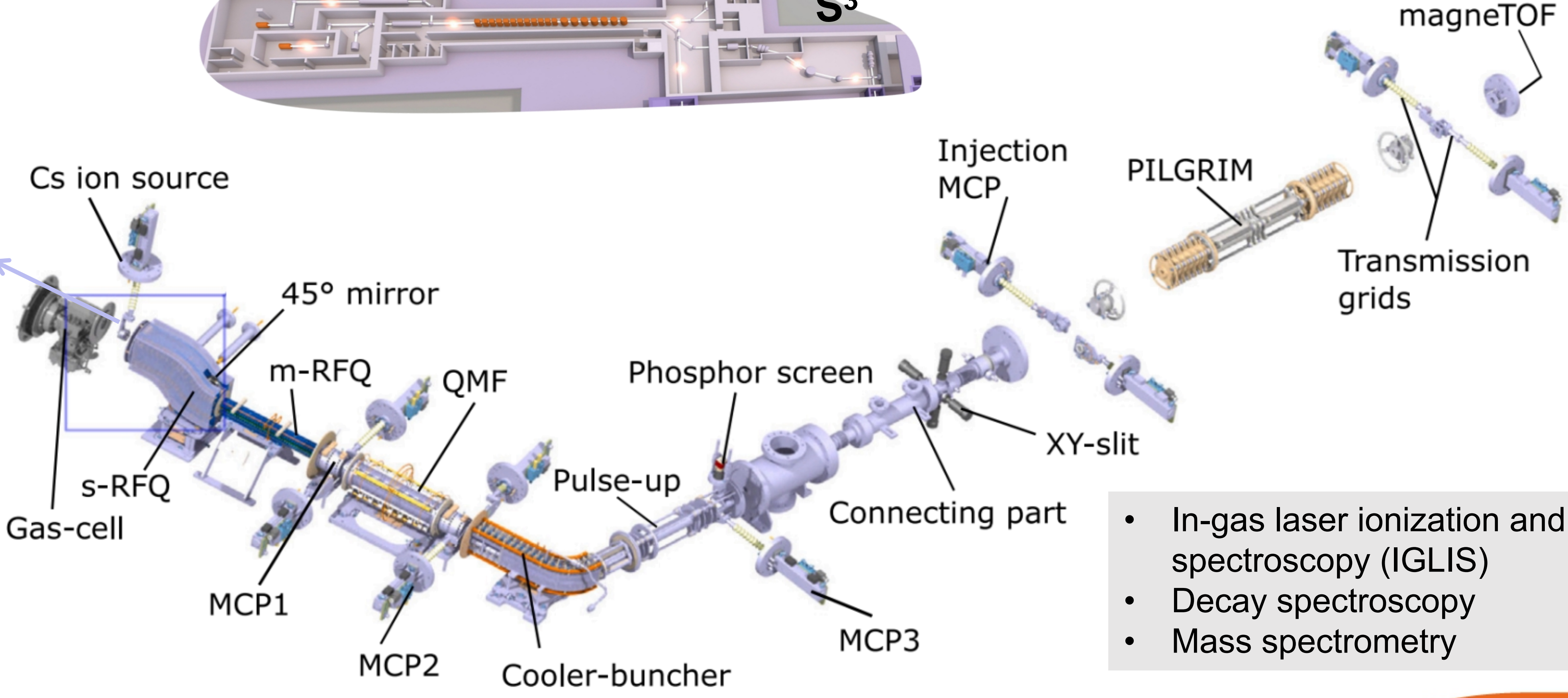

- In-gas laser ionization and spectroscopy (IGLIS)
- Decay spectroscopy
- Mass spectrometry

S³-LEB laser spectroscopy technique

Stop, neutralize in the gas cell and extract the atoms

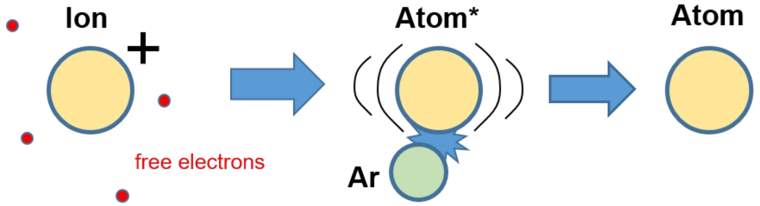

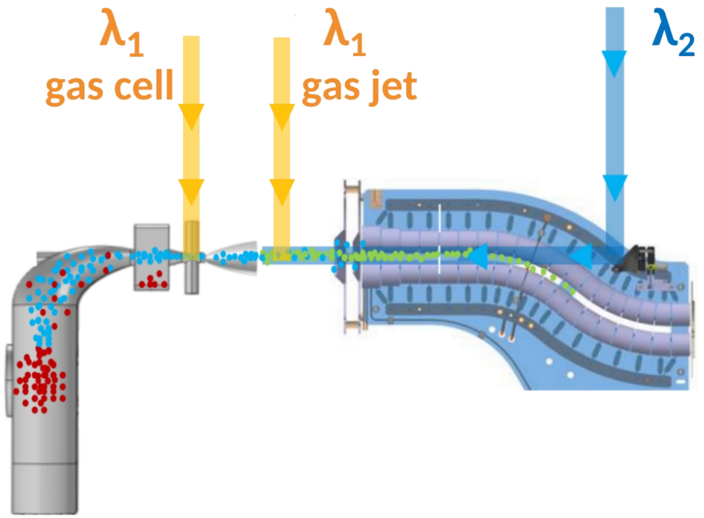

In-Gas Laser Ionization and Spectroscopy (IGLIS) technique with NB Ti:sa system

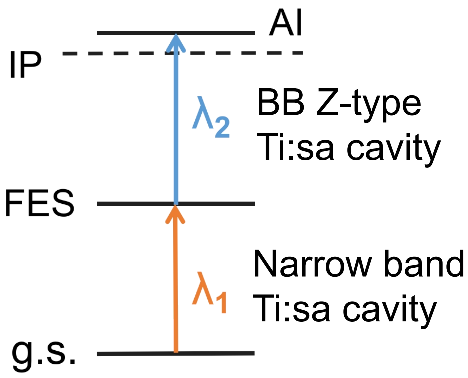

High-resolution in-gas-jet laser spectroscopy

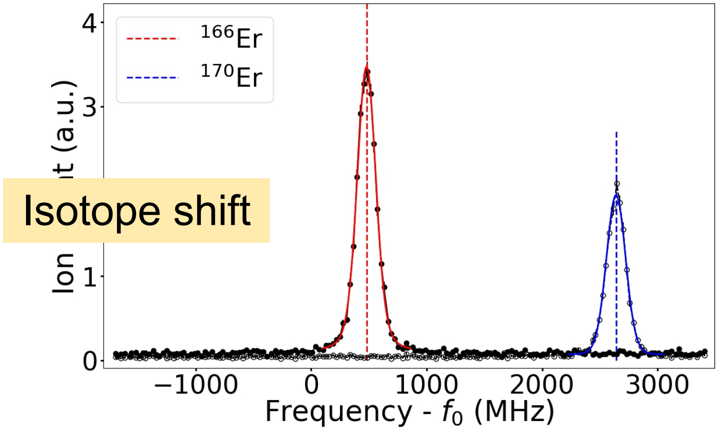

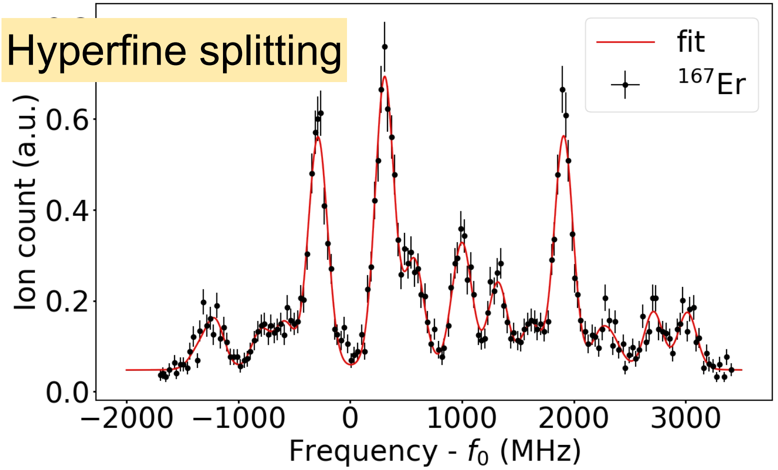

Nuclear properties

spin, moments and difference in mean-square charge radii...

General status of S3-LEB

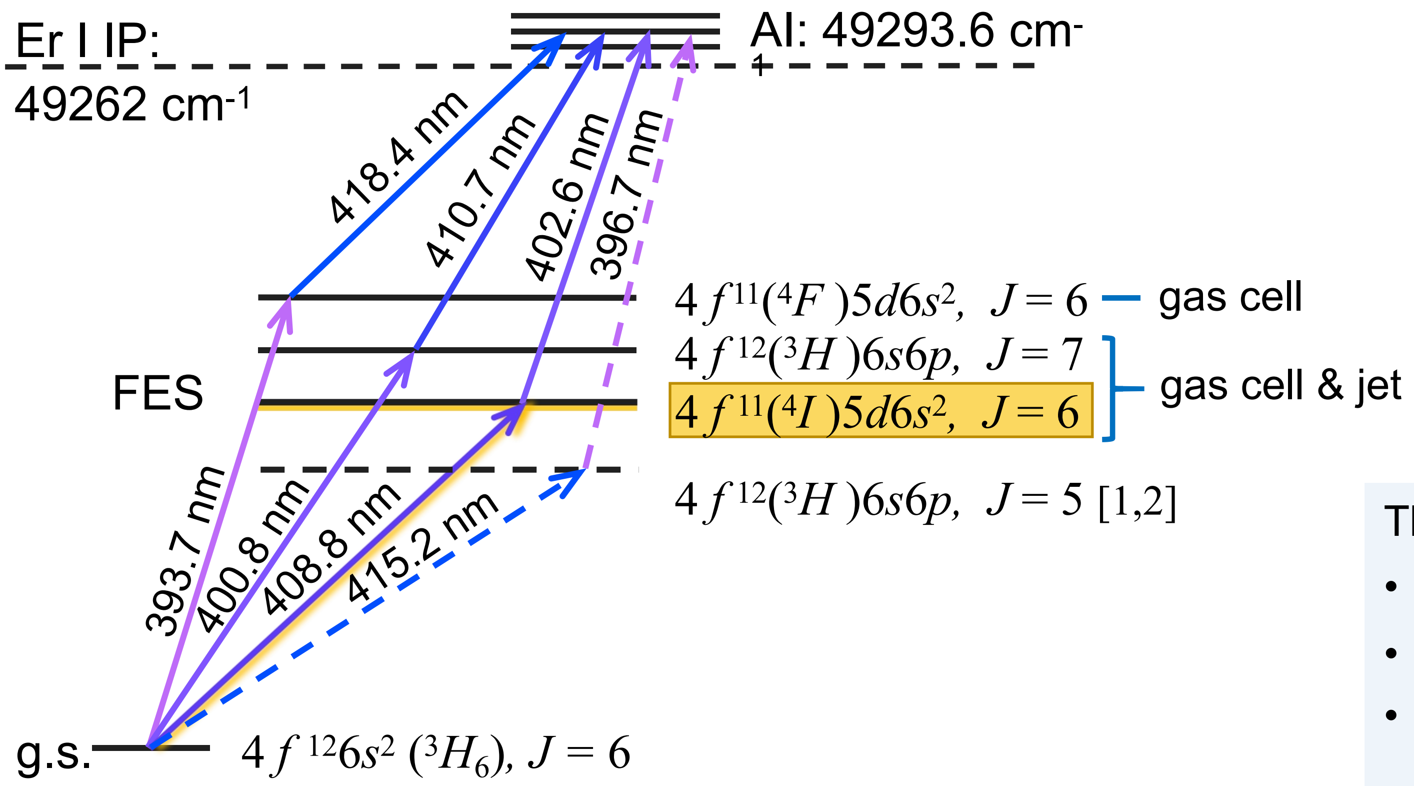

First commissioning case 415.2 nm

415 nm FES	Method	A (MHz)	B (MHz)
$4f^{12}(^3H_5)$ 6s6p, J=5	gas jet [1,2]	−147.1(7)	−1936(24)
	ref [3]	−146.6(3)	−1874(16)

Three different Er schemes explored in this work:

- 408.8 nm with injection-locked Ti:sa in gas jet.
- 400.8 nm with dual-etalon Ti:sa in gas jet.
- 408.8 nm, 400.8 nm, 393.7 nm with dual-etalon Ti:sa in gas cell.

[1] A. Ajayakumar et al.Nuclear Inst. and Methods in Physics Research, B 539 (2023)
[2] J. Romans et al. Nucl. Instrum. Meth. B 536 (2023)
[3] W.J. Childs et al., Phys. Rev. A 28 (1983)

Isotope shift extraction

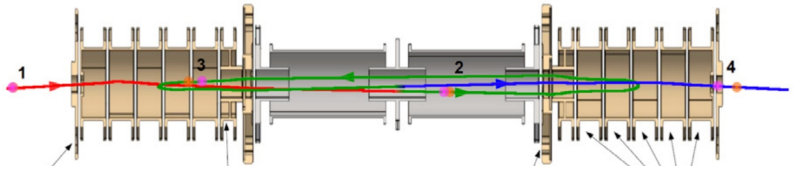

TOF spectrum after PILGRIM

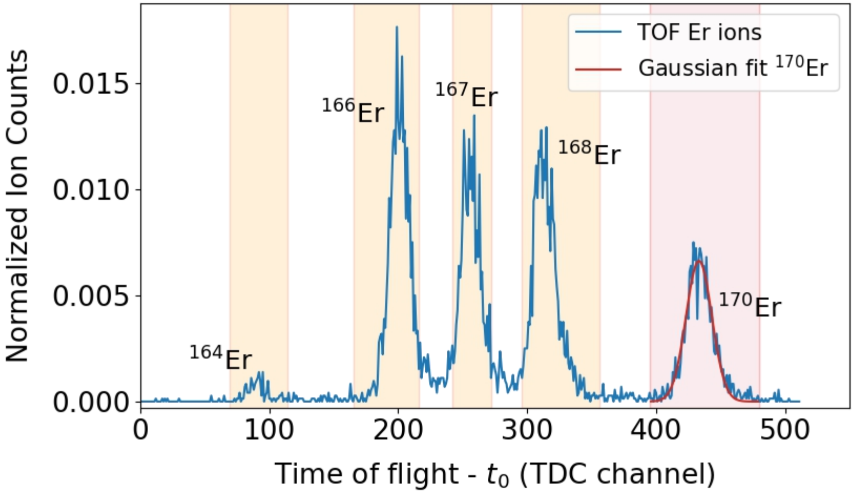

TOF gates range: 30 - 70 ns

408.8 nm gas cell

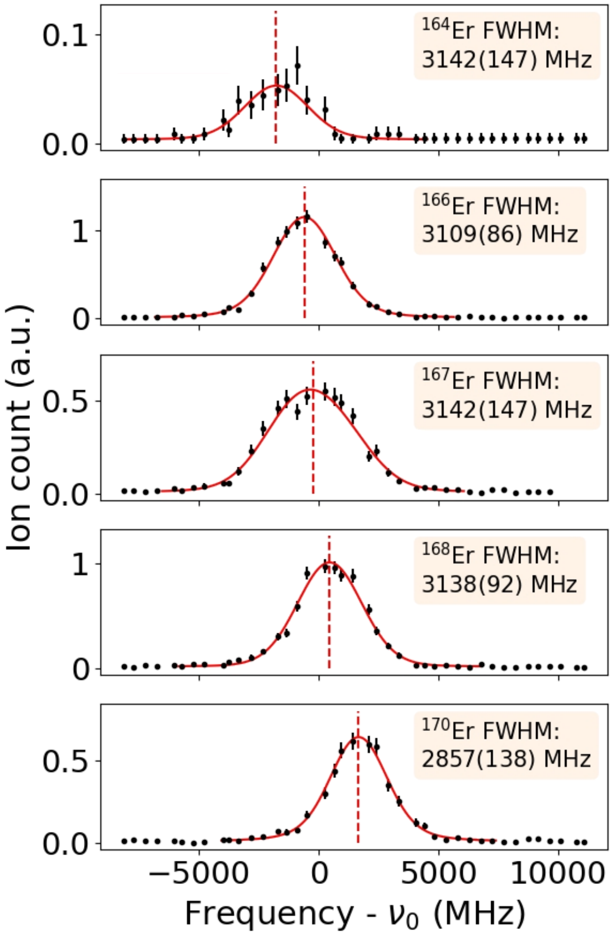

408.8 nm gas jet

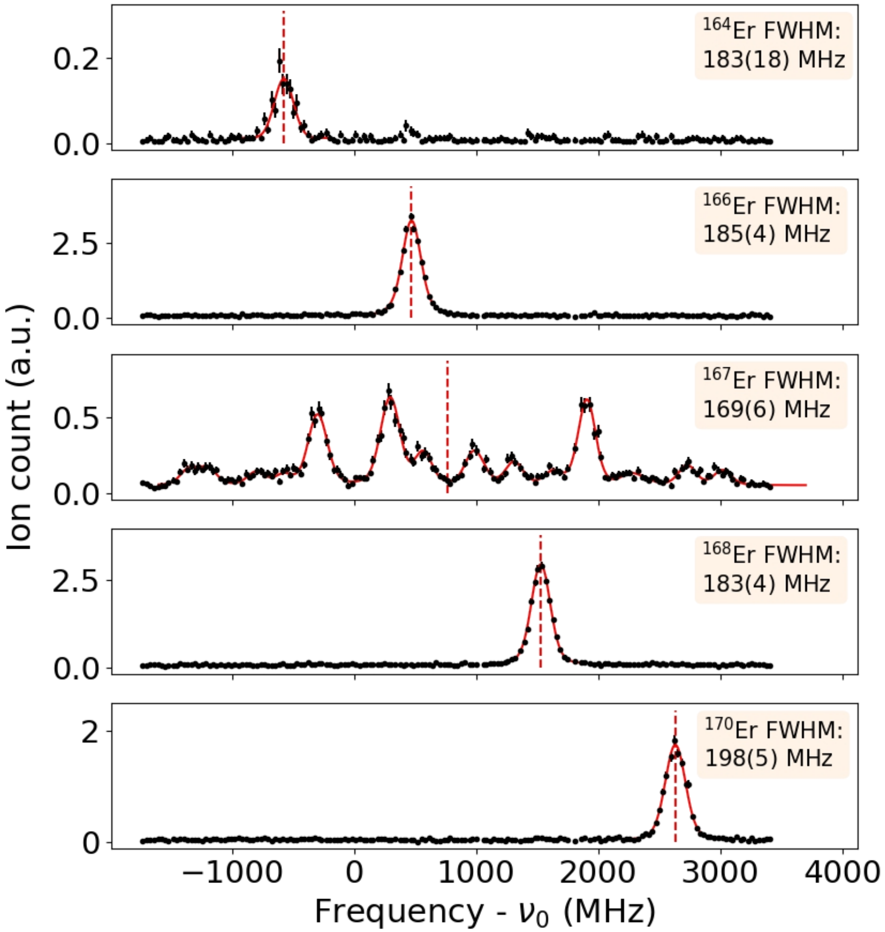

Isotope shift extraction

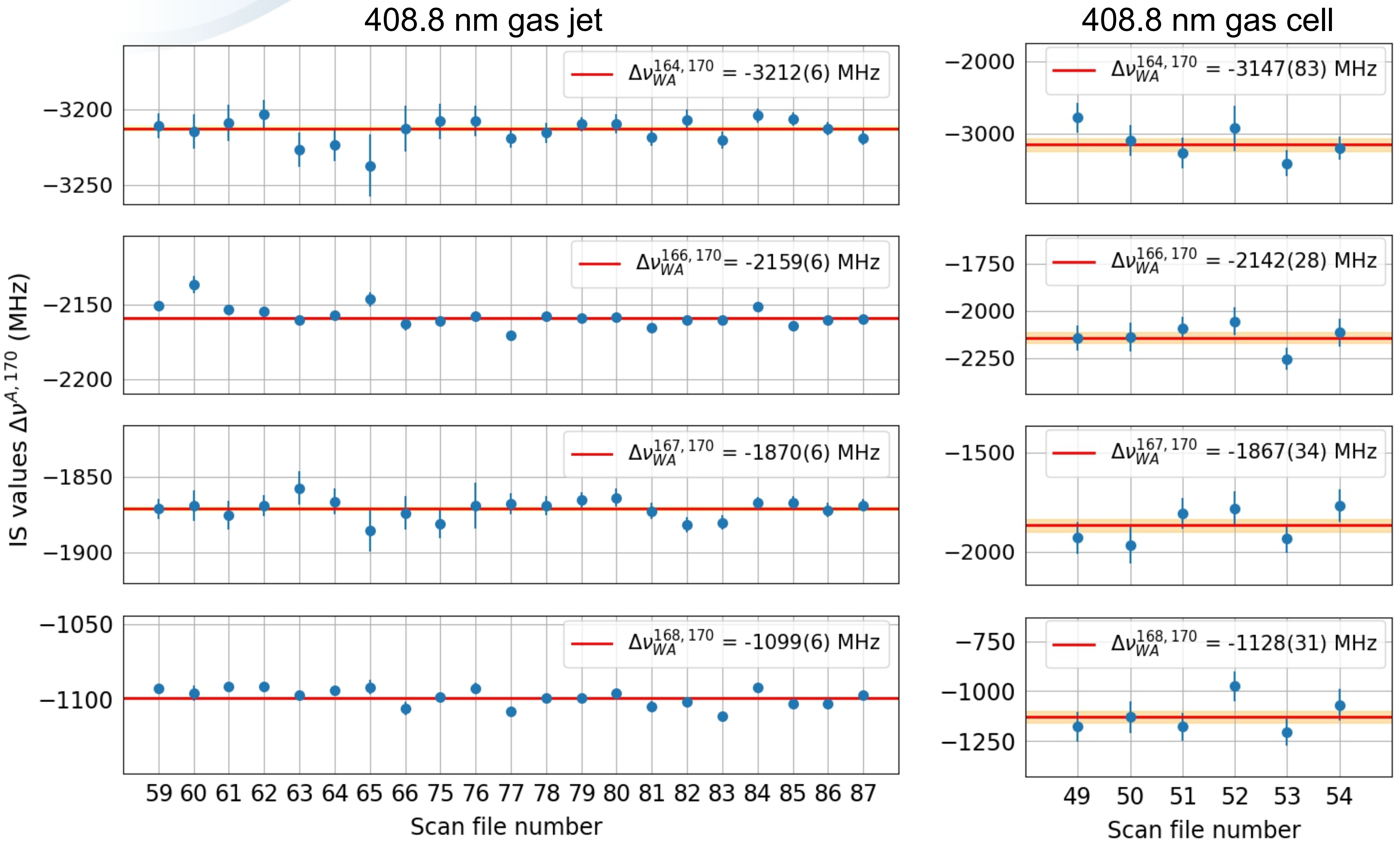

A'	Isotope shifts (MHz) $\Delta\nu^{A',170}_{WA}$	
	408.8 nm	
	gas cell	gas jet
164	-3147(83)	-3212(6)
166	-2142(28)	-2159(6)
167	-1867(34)	-1870(6)
168	-1128(31)	-1099(6)

King plot analysis

$$\delta\nu_i^{A',A} = F_i \delta\langle r^2\rangle^{A',A} + M_i \frac{A'-A}{A'A}$$

- Field shift: large F_i values → high sensitivity to $\delta\langle r^2\rangle^{A',A}$
- Mass shift: $M_i = M_{i,\mathrm{NMS}} + M_{i,\mathrm{SMS}}$

$$M_{i,\mathrm{NMS}} = \frac{\nu_i}{1836.15}$$

↓ King plot

Atomic factors F_i and M_i

King plot analysis

$$\delta\nu_i^{A',A} = F_i\,\delta\langle r^2\rangle^{A',A} + M_i\frac{A'-A}{A'A}$$

- Field shift: large F_i values → high sensitivity to $\delta\langle r^2\rangle^{A',A}$
- Mass shift: $M_i = M_{i,\mathrm{NMS}} + M_{i,\mathrm{SMS}}$

$$M_{i,\mathrm{NMS}} = \frac{\nu_i}{1836.15}$$

King plot

Atomic factors F_i and M_i

Type I using muonic X-ray $\lambda^{A',170}$ data:

$$(\Delta\nu_i^{A',A})_{\mathrm{mod}} = F_i(\Lambda^{A',A})_{\mathrm{mod}} + \mu M_i$$

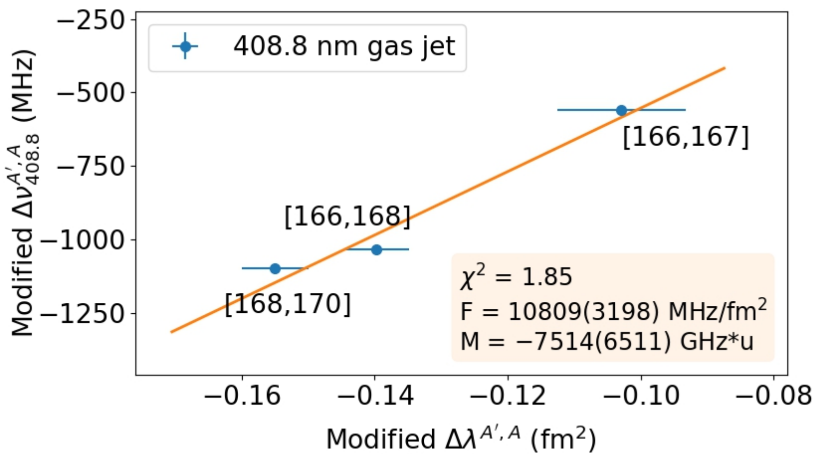

Limitations:

- Type I: too large uncertainties.

King plot analysis

$$\delta\nu_i^{A',A} = F_i \delta\langle r^2\rangle^{A',A} + M_i \frac{A'-A}{A'A}$$

- Field shift: large F_i values → high sensitivity to $\delta\langle r^2\rangle^{A',A}$
- Mass shift: $M_i = M_{i,\mathrm{NMS}} + M_{i,\mathrm{SMS}}$

$$M_{i,\mathrm{NMS}} = \frac{\nu_i}{1836.15}$$

King plot

Atomic factors F_i and M_i

Type I using muonic X-ray $\lambda^{A',170}$ data:

$$(\Delta\nu_i^{A',A})_{\mathrm{mod}} = F_i(\Lambda^{A',A})_{\mathrm{mod}} + \mu M_i$$

Type II using 583 nm reference:

$$(\Delta\nu_i^{A',A})_{\mathrm{mod}} = \frac{F_i}{F_{ref}}(\Delta\nu_{ref}^{A',A})_{\mathrm{mod}} + M_i - \frac{F_i}{F_{ref}}M_{ref}$$

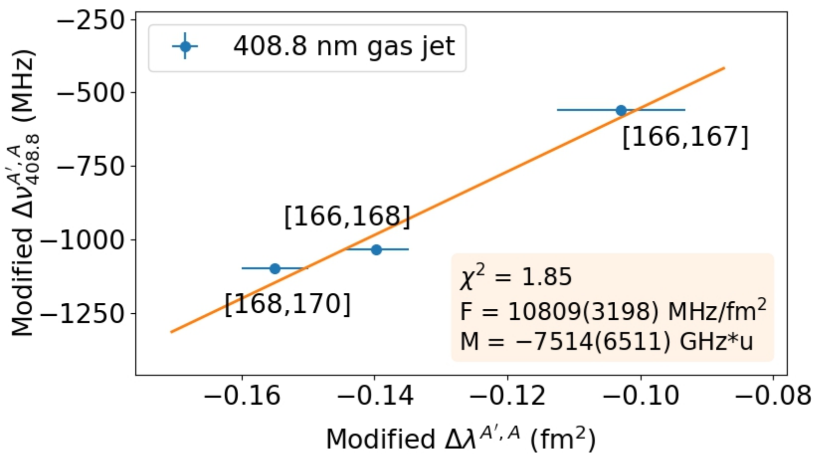

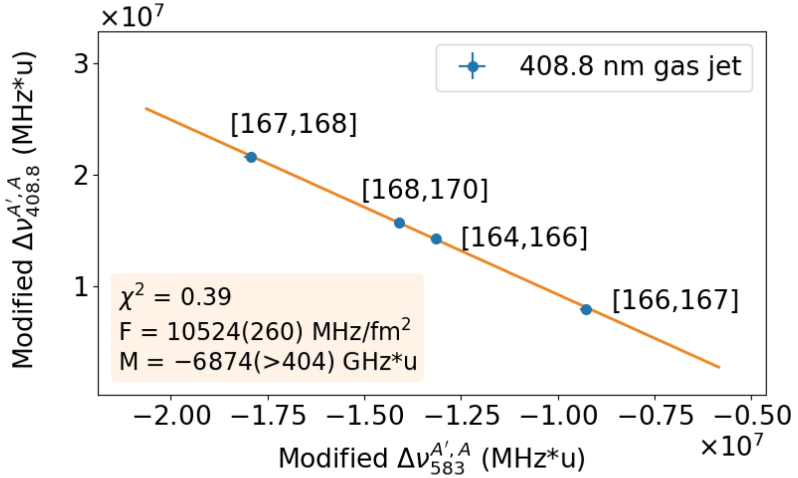

Limitations:

- Type I: too large uncertainties.

King plot analysis

$$\delta\nu_i^{A',A} = F_i \delta\langle r^2\rangle^{A',A} + M_i \frac{A'-A}{A'A}$$

- Field shift: large F_i values → high sensitivity to $\delta\langle r^2\rangle^{A',A}$
- Mass shift: $M_i = M_{i,\mathrm{NMS}} + M_{i,\mathrm{SMS}}$

$$M_{i,\mathrm{NMS}} = \frac{\nu_i}{1836.15}$$

⇩ King plot

Atomic factors F_i and M_i

Type I using muonic X-ray $\lambda^{A',170}$ data:

$$(\Delta\nu_i^{A',A})_{\mathrm{mod}} = F_i (\Lambda^{A',A})_{\mathrm{mod}} + \mu M_i$$

Type II using 583 nm reference:

$$(\Delta\nu_i^{A',A})_{\mathrm{mod}} = \frac{F_i}{F_{ref}} (\Delta\nu_{ref}^{A',A})_{\mathrm{mod}} + M_i - \frac{F_i}{F_{ref}} M_{ref}$$

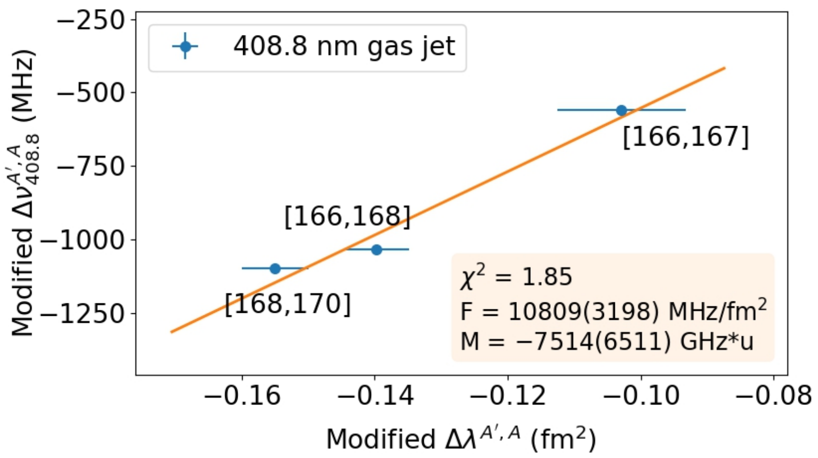

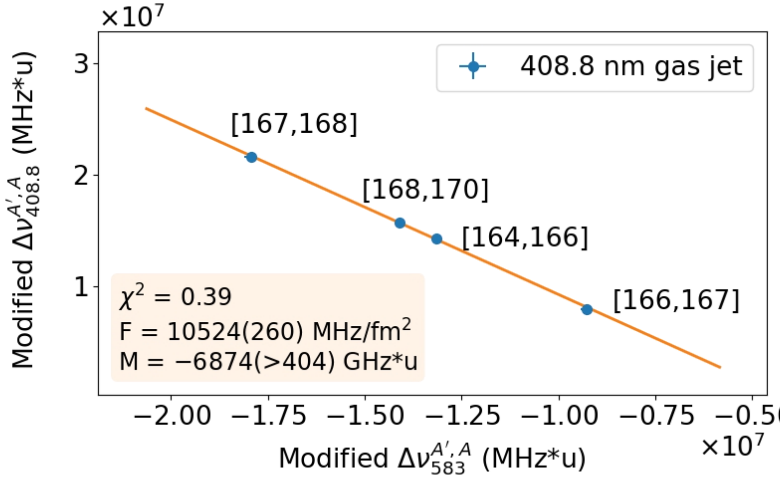

Limitations:

- Type I: too large uncertainties.
- Type II: the 583 nm reference[1] assuming $M_{i,\mathrm{SMS}} = 0$.

$$\delta\nu_{i,\ \mathrm{SMS}}^{A',A} = (0. \pm 0.5)\delta\nu_{i,\ \mathrm{NMS}}^{A',A}$$
for $ns^2 - nsnp$ transitions

[1] H. Okamura, S. Matsuki, Phys. Rev. C 35 (1987)

King plot with SMS estimation

$$\delta\nu^{A',A}_{i,\ \mathrm{SMS}} = (0. \pm 0.5)\delta\nu^{A',A}_{i,\ \mathrm{NMS}}$$
for $ns^2 - nsnp$ transitions

Intercept of type I King plot

$\mu M_i = \mu M_{i,\mathrm{NMS}}$ $(\pm\, 0.5\mu M_{i,\mathrm{NMS}})$

400.8 nm $6s^2$-$6s6p$, J=6-7 √

415.2 nm $6s^2$-$6s6p$, J=6-5 X

Type I King plot + SMS estimation for 400.8 nm and 415.2 nm

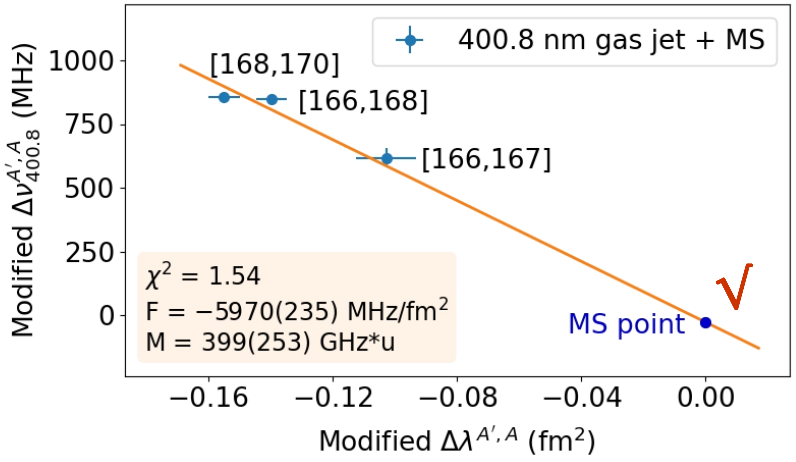

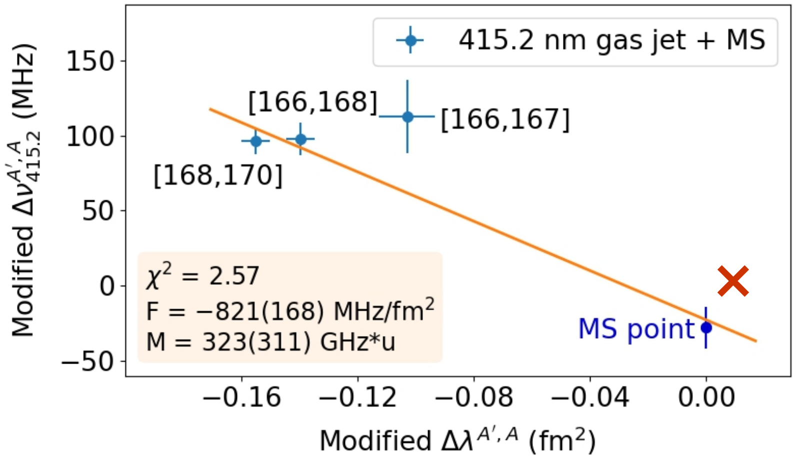

King plot with SMS estimation

Type I King plot + SMS estimation for 400.8 nm and 415.2 nm

$$\delta\nu_{i,\ \mathrm{SMS}}^{A',A} = (0. \pm 0.5)\delta\nu_{i,\ \mathrm{NMS}}^{A',A}$$
for $ns^2 - nsnp$ transitions

Intercept of type I King plot

$\mu M_i = \mu M_{i,\mathrm{NMS}}$ ($\pm\ 0.5\mu M_{i,\mathrm{NMS}}$)

400.8 nm 6s^2-6s6p, J=6-7 √

415.2 nm 6s^2-6s6p, J=6-5 X

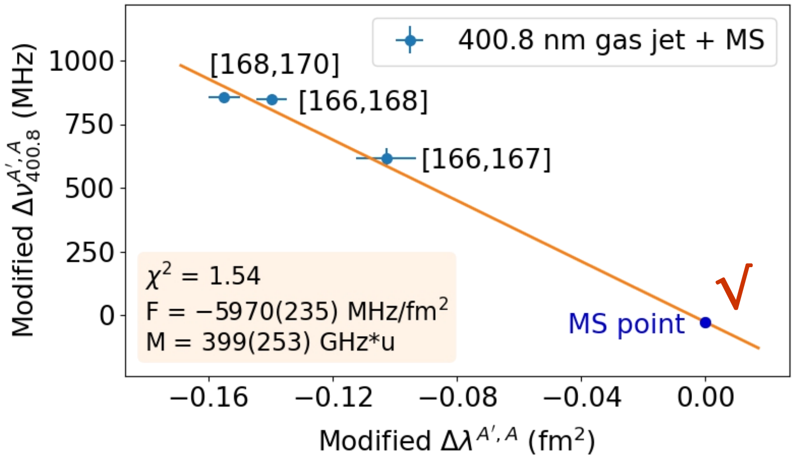

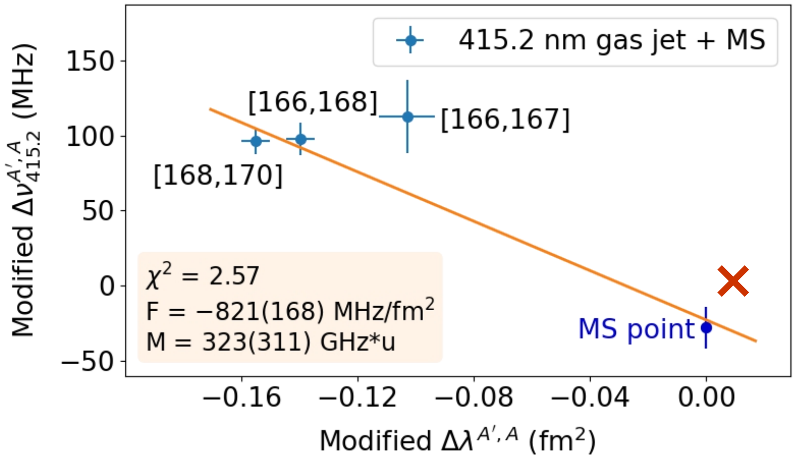

Reference 582.7 nm 6s^2-6s6p, J=6-7 theoretical calculation[5]

Atomic states	E_k (cm^{-1})		A (MHz)		B (MHz)		F (GHz/fm^2)
	Expt.	Calc.	Expt.	Calc.	Expt.	Calc.	Calc.
GS	0	0	-120.487	-120.66	-4552.984	-4880	-507.58
OS_{583}	17157	17392	-172.5	-164.3	-4440	-4602	-510.68

	Recent calc. [5]	[6] with *SMS* = 0
F_{583} (GHz/fm^2)	– 3.10	– 6.71(0.17)

Outlook: redo the King plot for 583 nm transition with calculated F_{583}

[5] V. Dzuba, V. Flambaum. UNSW.
[6] H. Okamura and S. Matsuki. Phys. Rev. C 35 (1987)

Spectral linewidths broadening mechanisms

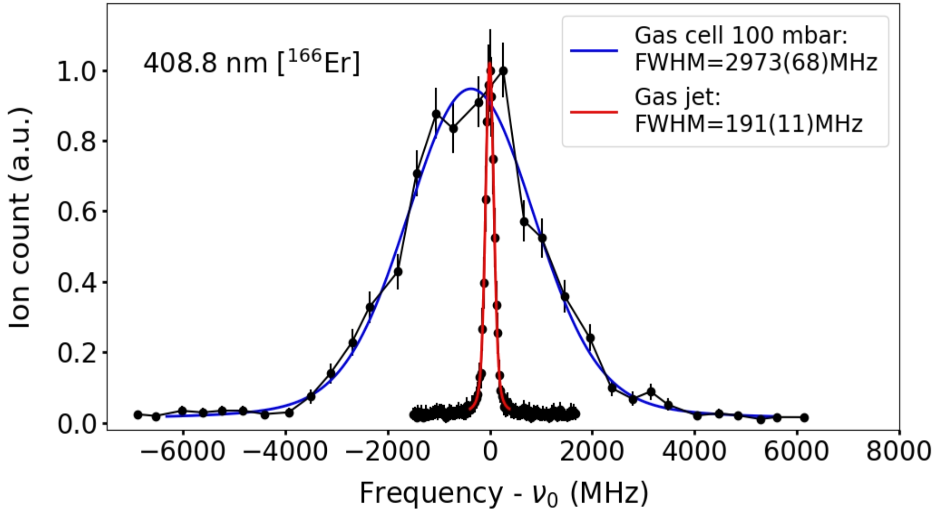

What are the factors causing the different linewidths?

- injection-locked Ti:sa in gas jet ~ 200 MHz
- dual-etalon Ti:sa in gas cell ~ 3GHz at 100 mbar

Power broadening of spectral linewidths

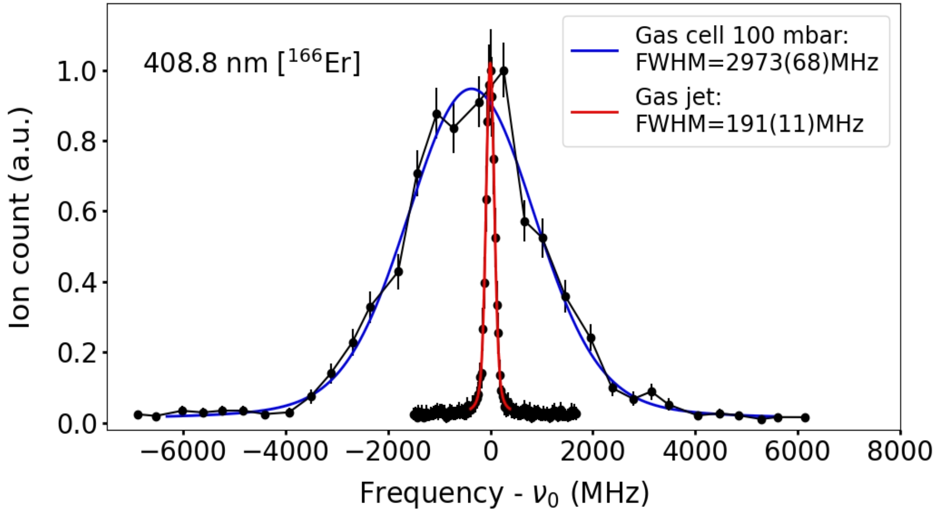

What are the factors causing the different linewidths?

- injection-locked Ti:sa in gas jet ~ 200 MHz
- dual-etalon Ti:sa in gas cell ~ 3GHz at 100 mbar

Power saturation test

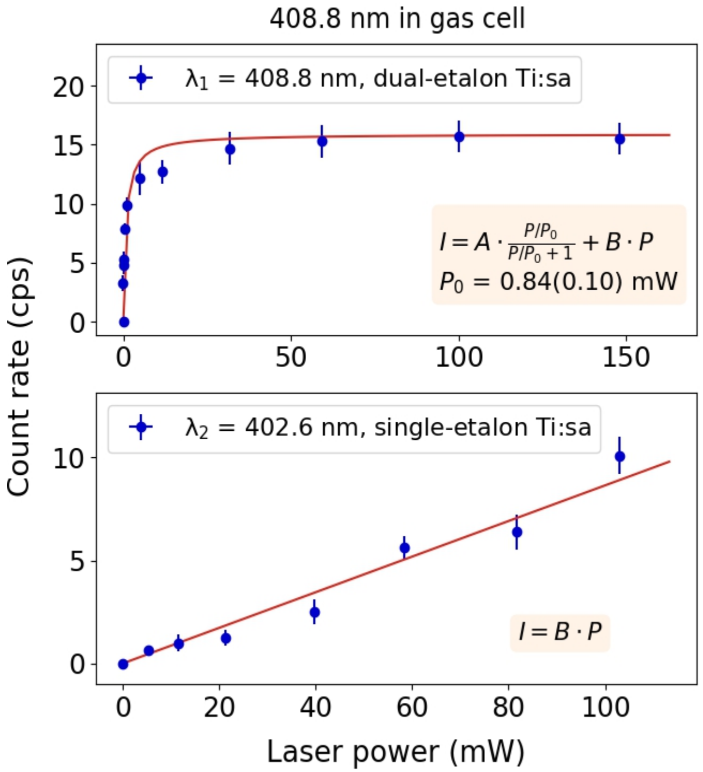

λ_1 easily saturated at mW.

λ_2 the AI transition, far from saturation.

Collisional broadening and shift of spectral lines

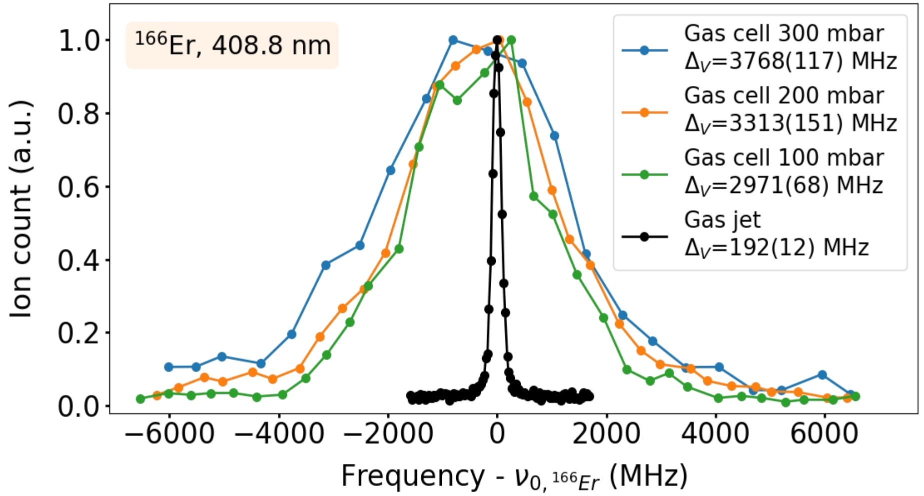

Collisional broadening and shift of spectral lines

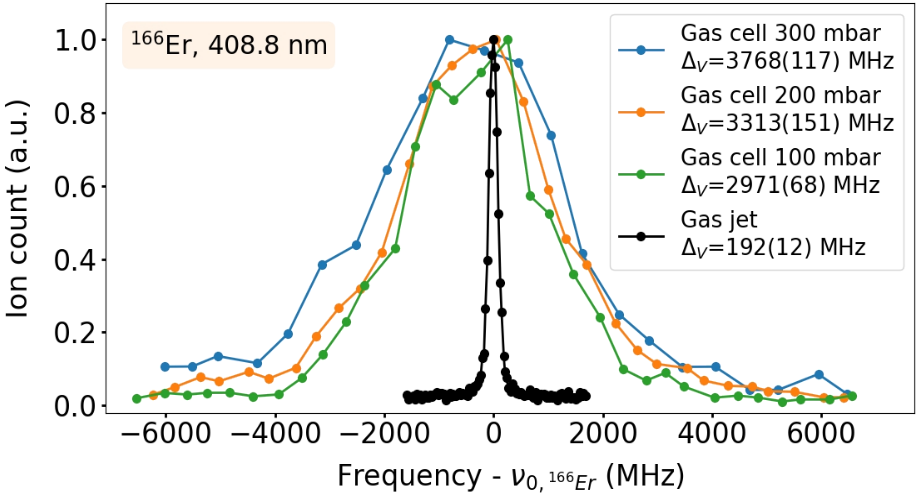

Excitation step (nm)	Broadening coef. (MHz/mbar)	Shift coef. (MHz/mbar)
408.8	4.53(0.66)	-0.13(0.29)
400.8	19.32(1.00)	-1.95(0.32)
415.2 [1]	11(1)	−4(1)

Collisional broadening and shift for ^{166,168,170}Er at different pressures

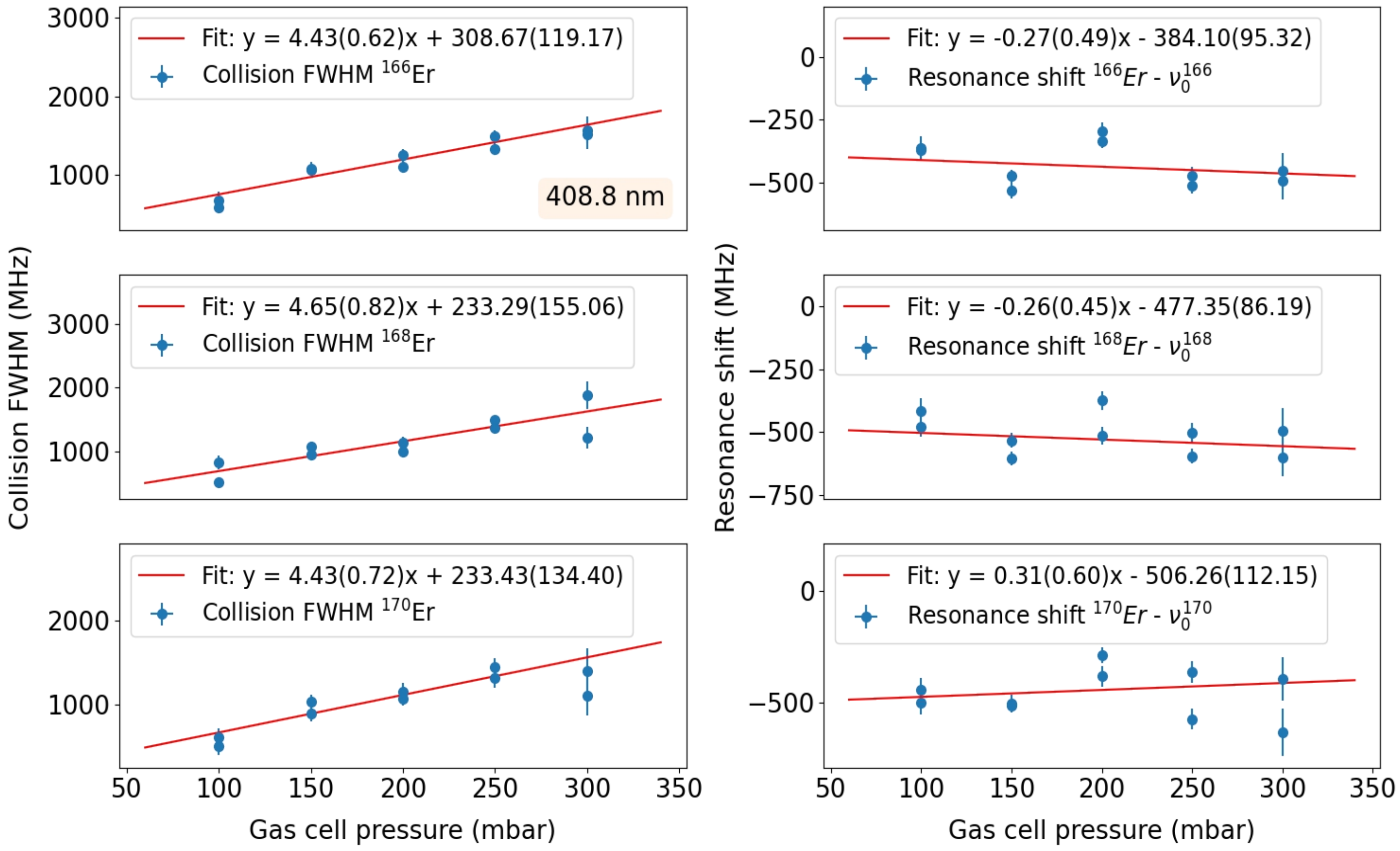

[1] A. Ajayakumar et al.Nuclear Inst. and Methods in Physics Research, B 539 (2023)

Hyperfine values for 408.8 nm FES

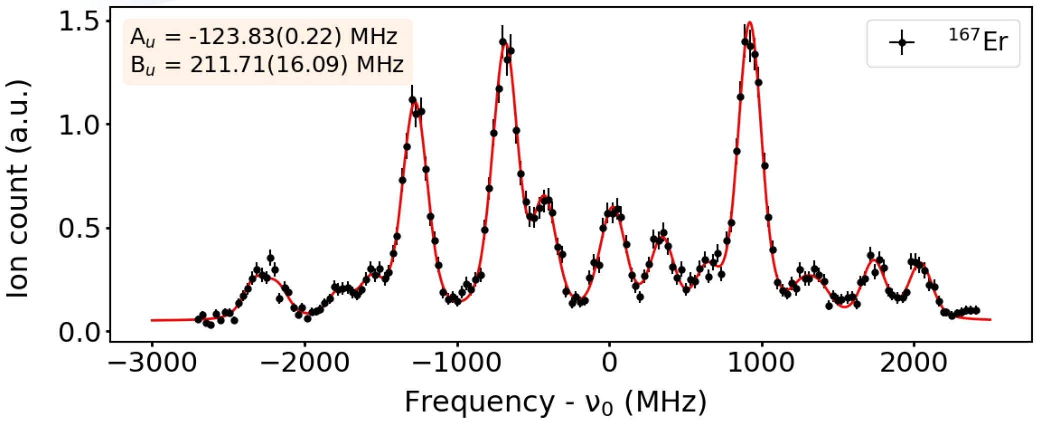

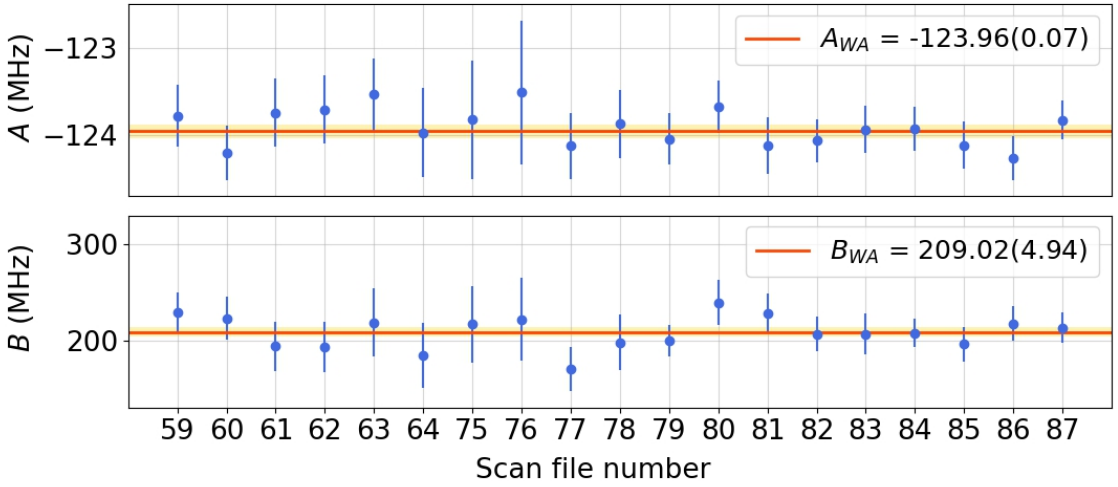

Hyperfine structure constants A and B for different FES of ^{167}Er

Atomic states	Excitation step(nm)	Method	A(MHz)	B(MHz)
$4f^{11}(^4I)5d6s^2$, J=6	408.8	gas jet	-124.0(6.0)	209.0 (7.8)
$4f^{12}(^3H_5)6s6p$, J=5	415.2	gas jet [1,2]	−147.1(7)	−1936(24)
g.s.	-	ref [3]	−121.8	−4563

[1] A. Ajayakumar et al.Nuclear Inst. and Methods in Physics Research, B 539 (2023)
[2] J. Romans et al. Nucl. Instrum. Meth. B 536 (2023)
[3] W.J. Childs et al., Phys. Rev. A 28 (1983)

Conclusion and outlook

Conclusion:

- The IS and HFS analysis of the 408.8 nm transition is finished. We found good agreement between gas-cell and gas-jet data. The transtion has large IS so is a good one for studying $\delta\langle r^2\rangle^{A',A}$, but it is challenging to get an accurate field shift factor from it.

Outlook:

- Try to include the theoretical calculation with experimental data to better constrain the F and M for the 408.8 nm transition.
- Next Step for S^3-LEB: more NB spectroscopy need to be done once the Matisse cavity is ready for the transitions that are not achievable with the current Ti:sa cavity.

Thank you for your attention!

GANIL:
Anjali Ajayakumar; Dieter Ackermann; Lucia Caceres; Samuel Damoy; Pierre Delahaye;
Patrice Gangnant; Nathalie Lecesne; Thierry Lefrou; Renan Leroy; Franck Lutton; Alejandro Ortiz;
Benoit Osmond; Julien Piot; Blaise-Maël Retailleau; Hervé Savajols; Gilles Sénécal

LPC:
Frédéric Boumard; Jean-François Cam; Philippe Desrues; Xavier Fléchard;
Julien Lory ; Yvan Merrer ; Christophe Vandamme

IJCLab:
Wenling Dong; Patricia Duchesne; Serge Franchoo; Vladimir Manea; Olivier Pochon

KU Leuven:
Arno Claessens; Rafael Ferrer; Mark Huyse; Fedor Ivandikov; Sandro Kraemer ; Yuri Kudriavtsev;
Jekabs Romans; Simon Sels; Paul Van den Bergh; Piet Van Duppen; Matthias Verlinde ; Elise Verstraelen

JGU:
Sebastian Raeder; Dominik Studer; Klaus Wendt

JYU:
Ruben de Groote; Iain David Moore; Michael Reponen; Juha Uusitalo

IPHC:
Emil Traykov

IRFU:
Martial Authier; Olivier Cloue; Antoine Drouard; Thomas Goigoux;
Emmanuel Rey-Herme; Damien Thisse; Marine Vandebrouck

and the RESIST network in ENSAR2

408.8nm

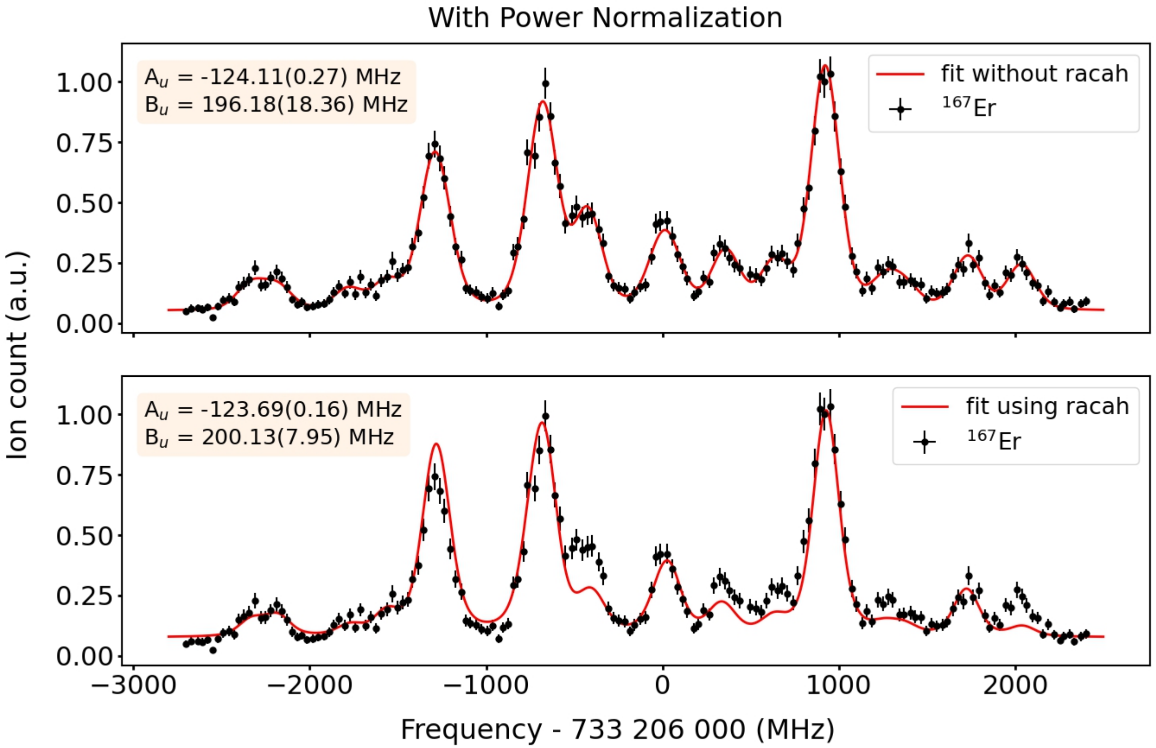

With Power Normalization
A_u = -124.11(0.27) MHz
B_u = 196.18(18.36) MHz
fit without racah
^{167}Er
A_u = -123.69(0.16) MHz
B_u = 200.13(7.95) MHz
fit using racah
^{167}Er
Ion count (a.u.)
Frequency - 733 206 000 (MHz)

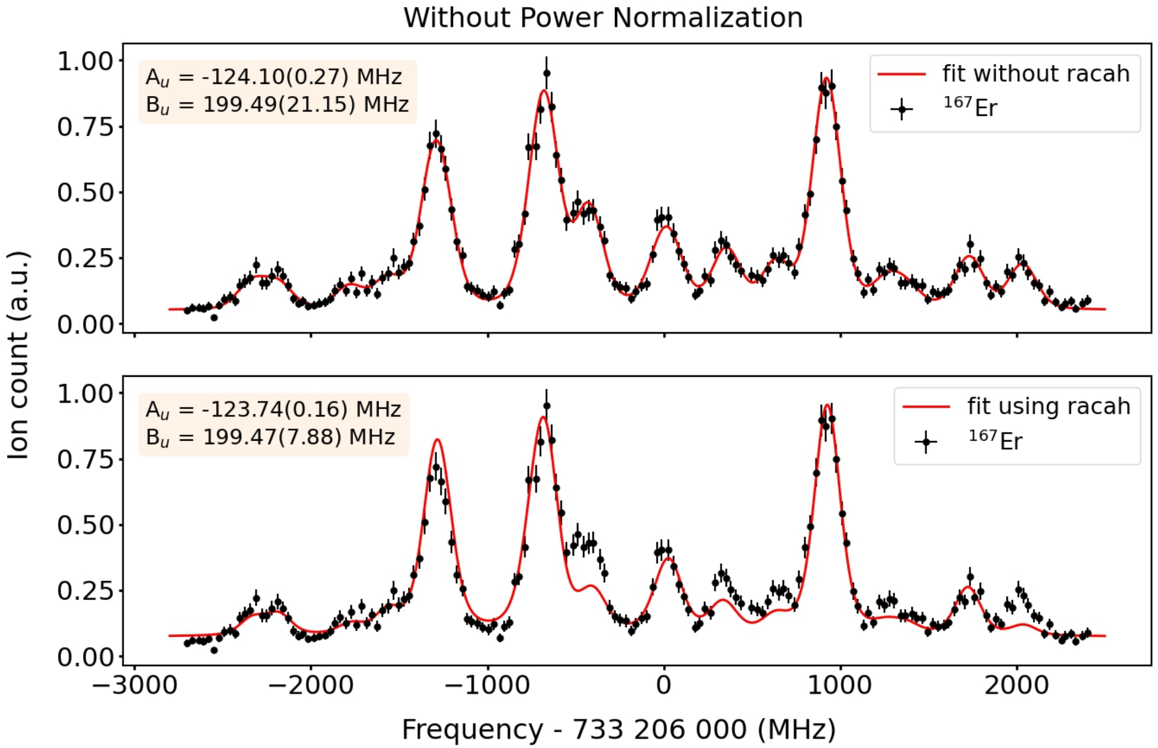

Without Power Normalization
A_u = -124.10(0.27) MHz
B_u = 199.49(21.15) MHz
fit without racah
^{167}Er
A_u = -123.74(0.16) MHz
B_u = 199.47(7.88) MHz
fit using racah
^{167}Er
Ion count (a.u.)
Frequency - 733 206 000 (MHz)

400.8nm IS studies

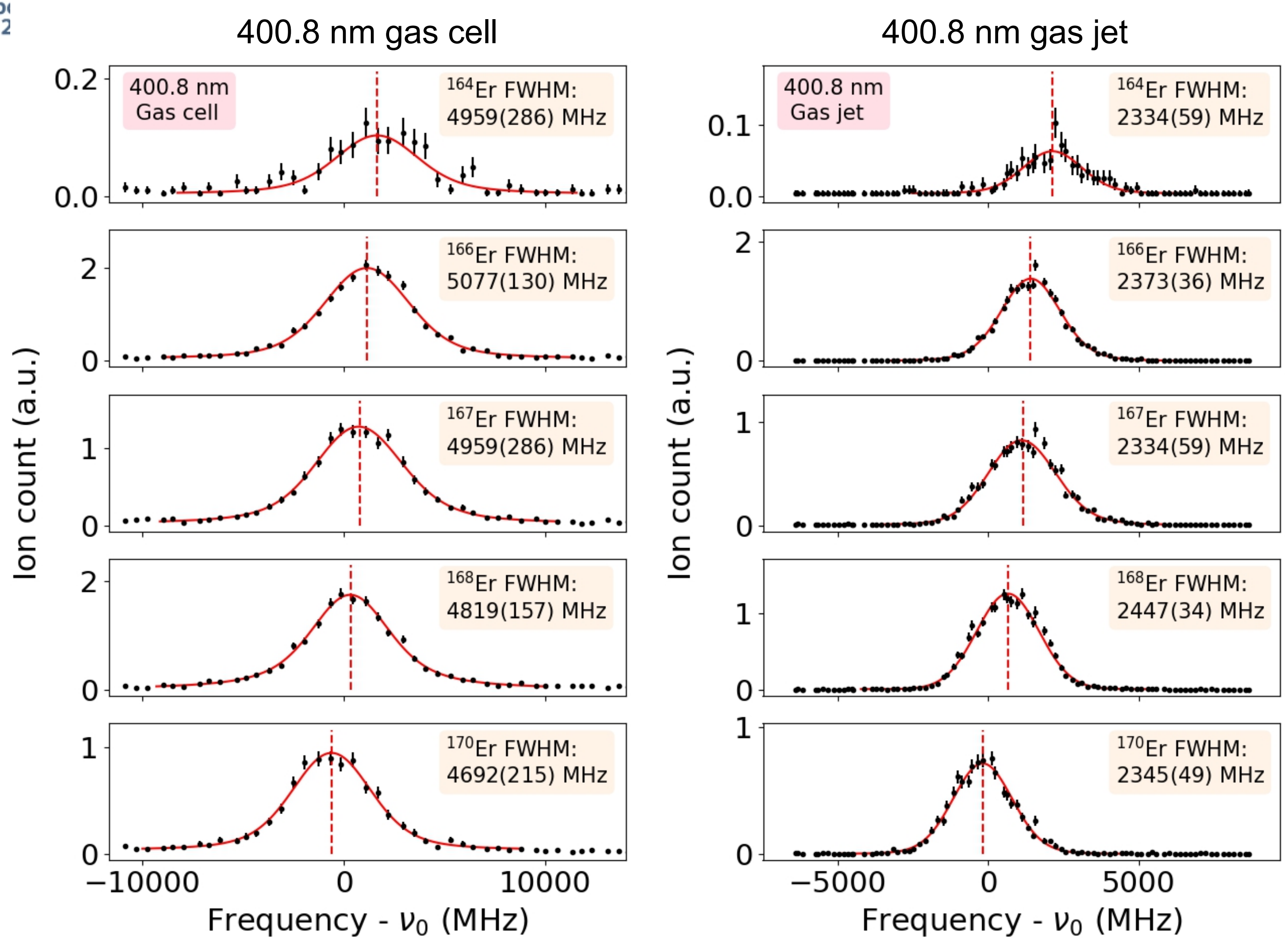

A'	Isotope shifts (MHz) $\Delta\nu_{\mathrm{WA}}^{A',170}$		
	400.8 nm		
	gas cell	gas jet	[4]
164	2386(118)	2517(39)	2530(22)
166	1748(44)	1720(43)	1681(14)
167	1415(38)	1395(29)	1384(15)
168	875(46)	855(13)	841(20)

[4] A. Frisch et al., Phys. Rev. A 88 (2013)

Spectral linewidths (FWHM)

Voight FWHM Δ_{voight}

- Gaussian linewidth Δ_G
  - Pulse linewidth $\Delta\nu_{pulse} = 441 / \tau_{pulse}$
  - Laser linewidth $\Delta\nu = \sqrt{2}\Delta\nu_{fundamental}$
  - Doppler brodening $\Delta\nu_{Doppler} = 7.16 \times 10^{-7} \nu_0 \sqrt{T / A}$
- Lorenztian linewidth Γ
  - Natural linewidth $\Gamma_{nat} = A / 2\pi$
  - Collisional brodening Γ_{coll}
  - Power brodening Γ_{power}

Can be calculated and fixed during the Satlas fit (pulse, laser, Doppler, natural linewidths)

Collisional brodening Γ_{coll} + Power brodening Γ_{power} **$= \Gamma - \Gamma_{nat}$**

$$\Delta_{voight} = 0.5346\Gamma + \sqrt{0.2166\Gamma^2 + \Delta_G^2}$$

$$\Delta_G = \sqrt{\Delta\nu_{pulse}^2 + \Delta\nu_{Doppler}^2 + \Delta\nu_{laser}^2}$$

$$\Gamma = \Gamma_{nat} + \Gamma_{coll} + \Gamma_{power}$$

408.8nm King plot analysis

IS = field shift + mass shift

Two types King plots

Atomic factors F_i and M_i

Large F_i values → high sensitivity to $\Lambda^{A',A} \approx \delta\langle r^2\rangle^{A',A}$.

Limitations:

- Type I: too large uncertainties.
- Type II: only reference for Er is the 583 nm transition[1] assuming $M_{i,SMS} = 0$.

Type I using muonic X-ray $\lambda^{A',170}$ data:

$$(\Delta\nu_i^{A',A})_{\text{mod}} = F_i(\Lambda^{A',A})_{\text{mod}} + \mu M_i$$

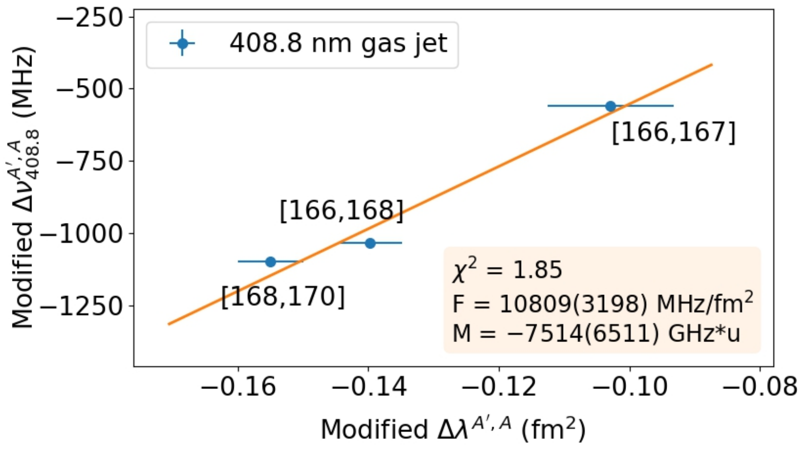

Type II using 583 nm reference:

$$(\Delta\nu_i^{A',A})_{\text{mod}} = \frac{F_i}{F_{ref}}(\Delta\nu_{ref}^{A',A})_{\text{mod}} + M_i - \frac{F_i}{F_{ref}}M_{ref}$$

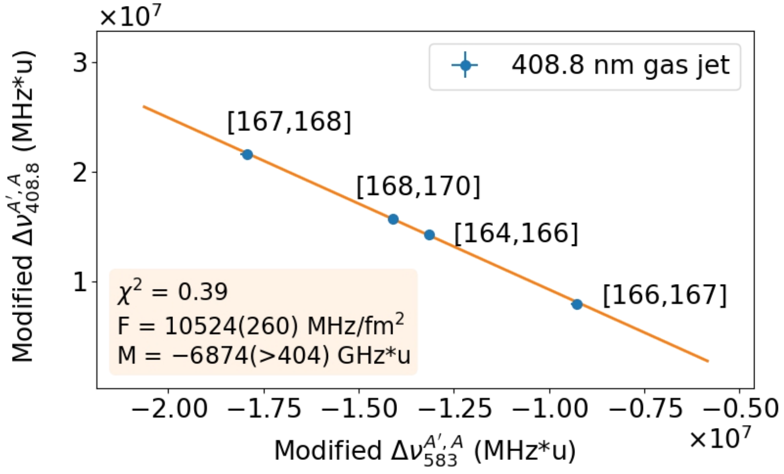

$M_i = M_{i,NMS} + M_{i,SMS}$

- $M_{i,NMS} = \dfrac{\nu_i}{1836.15}$
- $M_{i,SMS} = (0. \pm 0.5)\, M_{i,NMS}$ for ns^2-$nsnp$ transitions

$\delta\nu_{i,\,\text{SMS}}^{A',A} = (0. \pm 0.5)\delta\nu_{i,\,\text{NMS}}^{A',A}$ for $ns^2 - nsnp$ transitions

$M_{i,SMS} = (0. \pm 0.5)\, M_{i,NMS}$ for ns^2-$nsnp$ transitions

[1] H. Okamura, S. Matsuki, Phys. Rev. C 35 (1987)